Available online at www.sciencedirect.com

SciVerse ScienceDirect

Journal of the European Ceramic Society 32 (2012) 1321–1327

www.elsevier.com/locate/jeurceramsoc

Effect of sintering conditions and heat treatment on the properties, microstructure and machining performance of α-β-SiAlON ceramics

N. Calis Acikbas [a,*], H. Yurdakul [b], H. Mandal [b,d], F. Kara [b], S. Turan [b], A. Kara [b], B. Bitterlich [c]

[a] *MDA Advanced Ceramics Ltd., Eskisehir, Turkey*
[b] *Department of Materials Science and Engineering, Anadolu University, Eskisehir, Turkey*
[c] *Ceramtec AG, Plochingen, Germany*

Received 19 October 2011; accepted 22 November 2011
Available online 23 December 2011

Abstract

The properties of SiAlON ceramics are strongly affected by the composition and structure of the intergranular phase, which are controlled by dopants, sintering conditions and starting silicon nitride (Si_3N_4) powder characteristics. In this study, 25α:75β SiAlON compositions were designed with different molar ratios of Y:Sm:Ca (9:0.5:0.5 and 3:6:1). The effects of cation ratios, different cooling profiles (50 °C/min and 5 °C/min) and further heat treatment under different conditions (at 1600 °C for 2, 4 and 6 h) on the final phase composition, the type of the intergranular phase (amorphous or crystalline) formation, the resulting microstructures and the machining performance were studied. It is found that slow cooling and heat treatment have a great influence on crystallisation behaviour and in turn the crystallisation enhance the machining performance of SiAlON materials in cutting tool applications.

Keywords: SiAlON; Cation; Heat treatment; Crystallisation; TEM characterisation; Properties

1. Introduction

α-β-SiAlON and Si_3N_4 ceramics are used as a cutting tool material due to their high toughness and high hardness. Out of these two class of materials, α-β-SiAlON ceramics have some advantages over Si_3N_4 ceramics due to a combination of high hardness (20 GPa) resulting from the existence of α-SiAlON (α′: $Me_xSi_{12-(m+n)}Al_{m+n}O_nN_{16-n}$), a relatively high toughness (7–8 $MPam^{1/2}$) and strength (≥800 MPa) resulting from the β-SiAlON (β′: $Si_{6-z}Al_zO_zN_{8-z}$) phase. It is well known that microstructure evolution has an effect on the mechanical properties of SiAlON ceramics and the microstructure is influenced by the type of sintering additives, sintering conditions and type of the starting Si_3N_4 powder characteristics.[1–6] For this purpose, most of the research has been concentrated on the effect of sintering additives on grain growth and intergranular phases.[1–6] From all these studies, it is concluded that an increase in aspect ratio of the grains and hence enhanced fracture toughness can be achieved by preferred segregation of large cations (La^{3+}, Sm^{3+}, Ce^{3+}, etc.) on the prism planes of the grains. Also, oxygen rich intergranular phases were obtained by using smaller cations such as Lu^{3+} or Yb^{3+}, while nitrogen containing intergranular phases formed with larger cations (La^{3+}, Ce^{3+}, etc.).[7–9]

In a previous study, the effect of Yb and Ce/Sm cations and their mixtures with different molar ratio (1Yb:1Ce, 3Yb:1Ce, 3Yb:1Sm, 9Yb:1Ce and 9Yb:1Sm) on the intergranular phase crystallisation were investigated.[10] However, in the SiAlON literature, there is no in depth study on intergranular phase crystallisation by using multi cation system and their effect on the microstructure and machining performance of the SiAlON materials. Therefore, in the current study, the effect of multi cation dopant (Y, Sm and Ca) system with different ratios (9Y:0.5Sm:0.5Ca and 3Y:6Sm:1Ca) on the intergranular phase

* Corresponding author. Present address: Department of Mechanical and Manufacturing Engineering, Bilecik University, Bilecik, Turkey.
Tel.: +90 228 216 02 83; fax: +90 228 216 05 88.
E-mail addresses: ncalis@gmail.com, nurcan.acikbas@bilecik.edu.tr (N. Calis Acikbas).
[d] Now at Sabanci University, Istanbul, Turkey.

0955-2219/$ – see front matter.
doi:10.1016/j.jeurceramsoc.2011.11.030

crystallisation, microstructural development and machining performance was investigated.

2. Experimental studies and materials

High purity α-Si_3N_4 powder (E-10 grade, UBE Co. Ltd., Japan) with 1.4 wt% O content was mixed with high purity AlN powder (H Type, Tokuyama Corp., Japan) containing 1.6 wt% O, Al_2O_3 (Alcoa A16-SG, Pittsburgh, USA), Y_2O_3 (>99.9%, H.C. Starck Berlin, Germany), Sm_2O_3 (>99.9%, Stanford Materials Corp., USA) and $CaCO_3$ (>99.75%, Reidel-de Haen, Germany).

For Y–Sm–Ca multi cation system, CaO is used in order to avoid α → β SiAlON transformation, Y_2O_3 and/or Re_2O_3 (where Z_{Re}[3]62) to increase the stability and hardness of α-SiAlON and Sm_2O_3 (where $Z_{Re} < 62$) to develope elongated β-SiAlON grains and hence increase the fracture toughness.[11] 25α:75β SiAlON compositions were designed with different multi cation molar ratio (9Y:0.5Sm:0.5Ca and 3Y:6Sm:1Ca). The total amount of additives was kept constant at 3 mol%. The composition of the SiAlON in the sample with nominally $n = 1.3$ and $m = 1.25$ has a lower x value, as would be expected ($x = m/3 = 0.416$) and z value is 0.25.

These compositions were prepared by wet milling in isopropyl alcohol using Si_3N_4 media. The slurries were then dried in a rotary evaporator and sieved with a mesh size of 250 μm. The powders were uniaxially pressed under 25 MPa and subsequently cold isostatically pressed at 300 MPa to improve the green density. The pellets were sintered using a two-step gas pressure sintering cycle with maximum 2.2 MPa nitrogen gas pressure at 1940 °C for 1 h. 50 °C/min (fast cooling) and 5 °C/min (slow cooling) cooling profiles were applied. Sintered samples with fast cooling were afterwards heat treated at 1600 °C for 2, 4 and 6 h under flowing nitrogen atmosphere.

The type and amount of crystalline phases and the α-β-SiAlON phase ratios were determined by means of X-ray diffraction analyses (XRD-Rigaku Rint 2000, Tokyo, Japan). Although it is well documented how to calculate α:β content in Si_3N_4 based materials,[12] it is difficult to quantify crystalline melilite content. Therefore, to see the effect of melilite crystallisation, the relative amount of melilite phase (M^1: $Ln_2Si_{3-x}Al_xO_{3+x}N_{4-x}$) was calculated by dividing the M^1 peak intensity at the interplanar spacing of $d_{211} = 2.81$ Å with the β-SiAlON peak intensity at $d_{101} = 2.67$ Å. To avoid misleading interpretations due to the different scattering capabilities of SiAlON and melilite, the I_M/I_β ratios were only compared from the samples having similar α and β content.

Polished surfaces of the samples were examined in a scanning electron microscope (SEM-ZEISS Supra 50VP) by using backscattered electron imaging mode. Electron transparent samples for transmission electron microscope (TEM) investigations were prepared by cutting, polishing, dimpling and finally ion beam thinning (Baltec RES 101). The prepared samples were then coated (Baltec MED 020) with a thin carbon film and characterized to identify α-β-SiAlON polymorphs and secondary phase compositions via 200 kV field emission TEM (JEOL 2100F) attached with a high angle annular dark field scanning transmission electron microscope (STEM-HAADF) detector and an energy dispersive X-ray (EDX) spectrometer (JEOL JED-2300T).

The mechanical properties, in particular hardness and Vickers indentation fracture toughness of the samples were determined with Charles and Evans formula[13] by indenting the mirror polished surfaces with a load of 10 kg for 10 s using a Vickers hardness tester. At least 5 indentations were made for each sample.

For machining tests, samples were ground to ISO-geometry SNGN120716T02020, which is a chamfered block with a width of 12.7 mm and a height of 7.9 mm. Machining tests were performed on a grey cast iron (GJL-150) with a cutting speed of 1000 m/min, a feed rate of 0.5 mm/rev. and a cutting depth of 2.0 mm. Because of the work piece geometry, soft interrupted cutting conditions were preferred. At regular intervals, the test was interrupted to measure the width of the wear mark. The maximum cutting length was almost 6 km, which corresponds to a cutting time of app. 6 min. In another test, only the casting skin of a high-alloyed grey cast iron (GJL-250) was machined under continuous cutting conditions. Generally, the casting lot of the work pieces can have a great effect on the width of the wear mark. Thus, care had been taken always to use the same casting lot for each comparative test.

3. Results and discussion

3.1. XRD analysis

The effect of different molar ratios, different sintering conditions and heat treatment for multiple dopant system of Y–Sm–Ca on the phase formation are shown in Figs. 1–3 and summarised in Table 1. For different molar ratios, despite the fact that the alpha/beta ratio is similar (79/21) after fast cooling, crystalline melilite phase formation is much higher in 60 mol% ($I_M/I_\beta = 0.56$) than 5 mol% ($I_M/I_\beta = 0.1$) (Fig. 1 and Table 1). This is due to the low eutectic temperature and high nitrogen solubility in the Sm–Si–Al–O–N system.[14] Moreover, the viscosity of Sm Si–Al–ON liquids is less than the other lanthanide containing SiAlONs and this makes densification easier.[14]

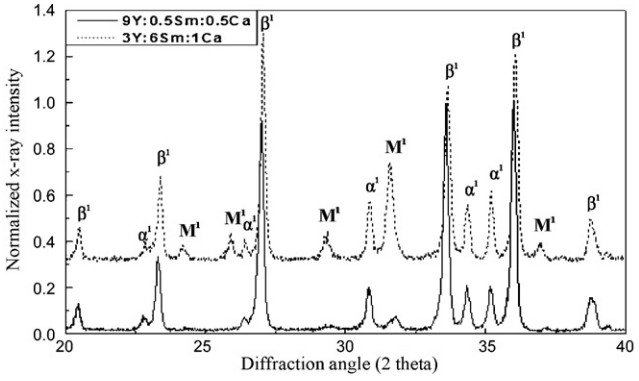

Fig. 1. XRD pattern showing the formation of rystalline phases after fast cooling of Y–Sm–Ca–SiAlONs containing different amount of dopant (β^1: beta SiAlON phase, α^1: alpha SiAlON phase, M^1: melilite phase ($Ln_2Si_{3-x}Al_xO_{3+x}N_{4-x}$)).

Table 1
Mechanical properties and phase evolution of SiAlON samples.

Molar content	Sintering conditions	HV10 (GPa)	Kıc (MPam$^{1/2}$)	α:β-SiAlON content (%)	Secondary phase	$I_{M^1}/I_{\beta'}$ ratio
3Y:6Sm:1Ca	Fast cooled	16.01 ± 0.23	5.89 ± 0.05	75β:25α	M^1 (vs)	0.56
	Fast cooled	15.70 ± 0.12	5.50 ± 0.02	79β:21α	M^1 (vw)	0.10
	Slow cooled	15.57 ± 0.14	5.43 ± 0.04	82β:18α	M^1 (s)	0.40
9Y:0.5Sm:0.5Ca	Heat treated at 1600 °C for 2 h	15.62 ± 0.20	5.65 ± 0.06	89β:11α	M^1 (s)	0.40
	Heat treated at 1600 °C for 4 h	15.55 ± 0.27	5.70 ± 0.05	90β:10α	M^1 (s)	0.42
	Heat treated at 1600 °C for 6 h	15.47 ± 0.30	5.73 ± 0.10	87β:13α	M^1 (s)	0.46

M^1: mellilite; s: strong; vs: very strong; vw: very week.

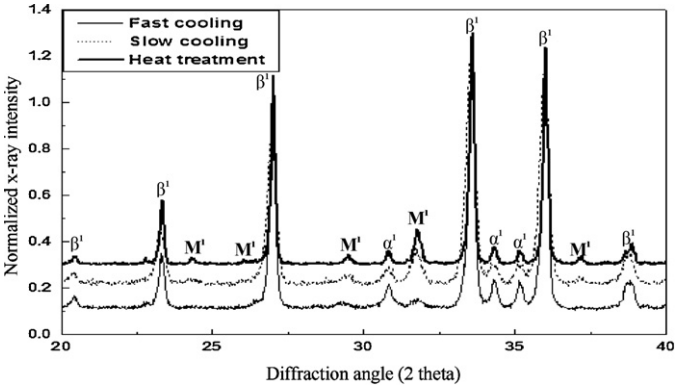

Fig. 2. Comparison of the crystallinity by fast cooling, slow cooling and heat treatment in Y–Sm–Ca containing system (heat treatment at 1600 °C for 2 h (β^1: beta SiAlON phase, α^1: alpha SiAlON phase, M^1: melilite phase ($Ln_2Si_{3-x}Al_xO_{3+x}N_{4-x}$)).

XRD results obtained for the fast and slow cooling and the heat treatment of Y-rich 9Y:0.5Sm:0.5Ca doped SiAlONs are given in Figure 2. During heat treatment and slow cooling some transformation took place and β-SiAlON content has increased to 89% and 82%, respectively (Table 1). The reason for increased amount of β-SiAlON is due to the fact that during heat treatment and slow cooling process, α-SiAlON stabilising cations released into the liquid phase, hence the amount of β-SiAlON phase increases.[15,16] More interestingly, a pronounced crystallisation of M^1 phase ($I_M/I_\beta = 0.4$) was observed after slow cooling or heat treatment whereas after fast cooling, only a very weak ($I_M/I_\beta = 0.1$) crystalline phase formation took place. It is important to note that crystalline phase to beta phase ratio is quite high despite the fact that the beta content increased after slow cooling and especially after heat treatment. Mandal and Thompson[17] showed the effect of sintering cooling profile on the intergranular phase crystallisation and they concluded that to achieve crystalline intergranular phase after sintering, cooling rate should be decreased from 30 °C/min to 3 °C/min. Slow cooling provides intergranular phase crystallisation without applying any post sintering heat treatment since it provides time for atoms to be regularly arranged. It was also reported by Thompson[18] that M^1 phase ($Ln_2Si_{3-x}Al_xO_{3+x}N_{4-x}$ where $0 \le x \le 1$) appeared at heat treatment temperatures in the range of 1450 °C to 1575 °C for Y and Sm densified SiAlONs, which is similar to the results obtained in this study. It can also be seen from Fig. 2 that slow cooling has almost the same effect as a heat treatment in terms of the amount of M^1 phase crystallisation ($I_M/I_\beta = 0.4$).

In order to evaluate the effect of heat treatment time on crystallisation, Y-rich samples were subjected to heat treatments for 2, 4 and 6 h (Fig. 3). Heat treatments at 1600 °C resulted in almost 5 times higher mellilite phase ratio compared to the fast cooled samples (Table 1). However, there was no difference in mellilite ratio (0.40–0.46) between 2 and 6 h of heat treatment times. This indicates that 2 h heat treatment is enough to obtain complete crystallisation of intergranular phase into M^1.

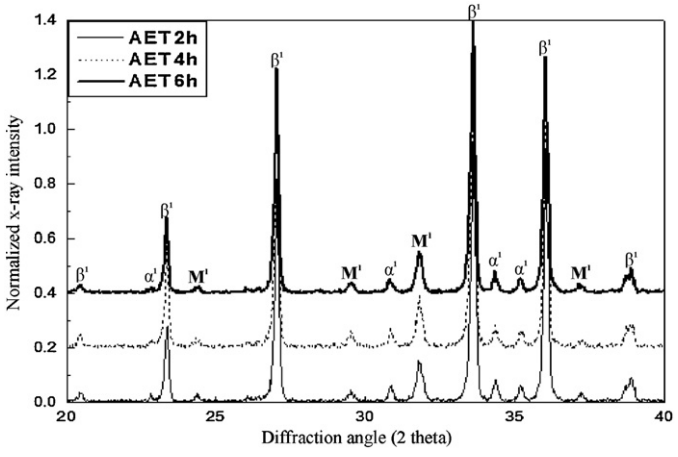

Fig. 3. Comparison of crystallinity after heat treatment at 1600 °C for 2, 4 and 6 h (β^1: beta SiAlON phase, α^1: alpha SiAlON phase, M^1: melilite phase ($Ln_2Si_{3-x}Al_xO_{3+x}N_{4-x}$)).

3.2. Microstructural development

In order to compare the microstructural differences after fast and slow cooling and heat treatment, typical back scattered SEM images of 9Y:0.5Sm:0.5Ca doped SiAlON are given in Fig. 4. There is not much difference about the microstructure for both slow and fast cooled samples (Fig. 4(a) and (b)), whereas heat treatment at high temperatures not only causes grain growth but also encourages the liquid phase to diffuse along grain boundaries and leads to coalescence of submicron triple junctions into larger pockets where crystallisation into M^1 readily occurred (Fig. 4(c)).

Fig. 5 shows TEM image of a crystalline triple junction phase in sintered sample. Based on the results shown in the image series of Fig. 5, the general microstructure of sintered Y–Sm–Ca doped SiAlON sample can be visualized as consisting of SiAlON grains and quadruples or triple junction points hosting for secondary phase formation that clearly seen (labelled with arrows "1" and "2" in (Fig. 5(a)). Considering HREM

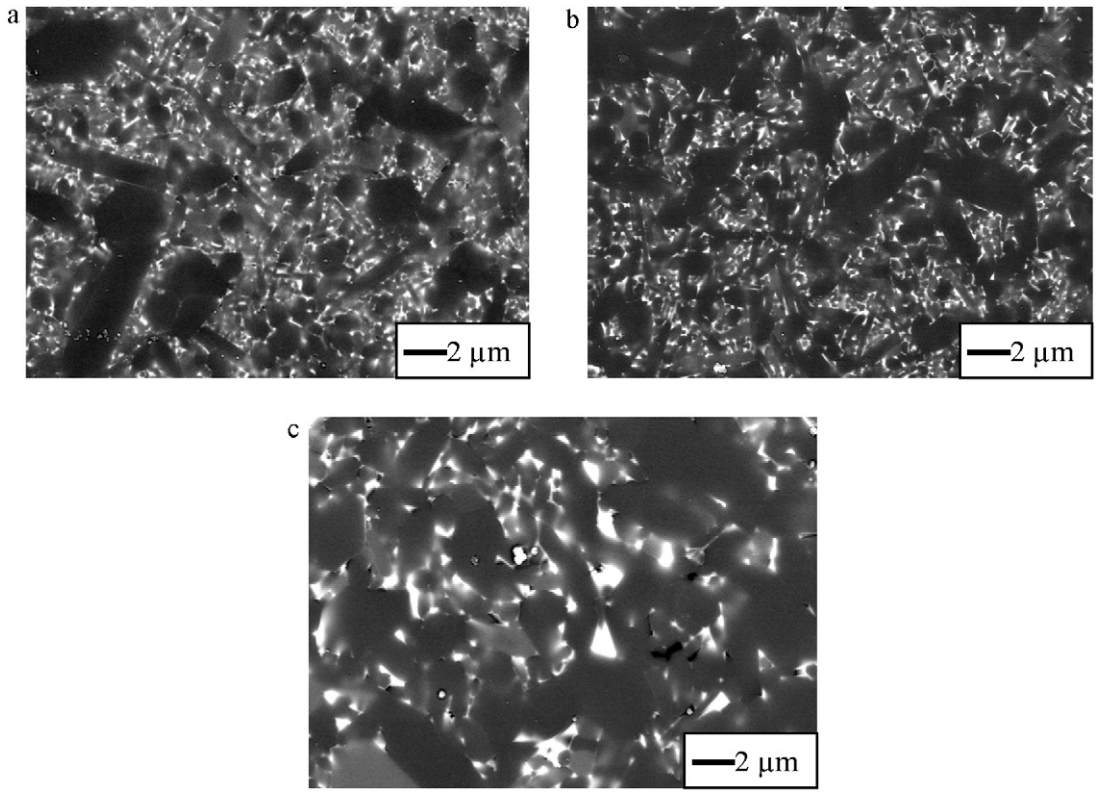

Fig. 4. Representative SEM images of Y–Sm–Ca doped SiAlONs after (a) fast cooling, (b) slow cooling and (c) heat treatment for 2 h.

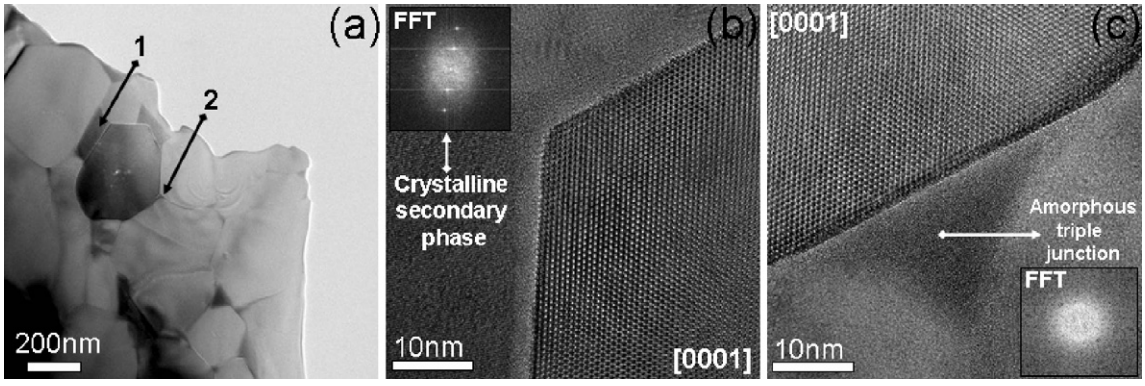

Fig. 5. (a) Representative TEM-BF image of sintered Y–Sm–Ca doped SiAlON sample, (b) HREM image of crystalline secondary phase labelled with "1" in panels (a) and (c) HREM image of amorphous triple junction region indicated by "2" in (a). Please note that insert figures in (b) and (c) correspond to fast Fourier transform (FFT) of crystalline secondary phase and amorphous triple junction region, respectively.

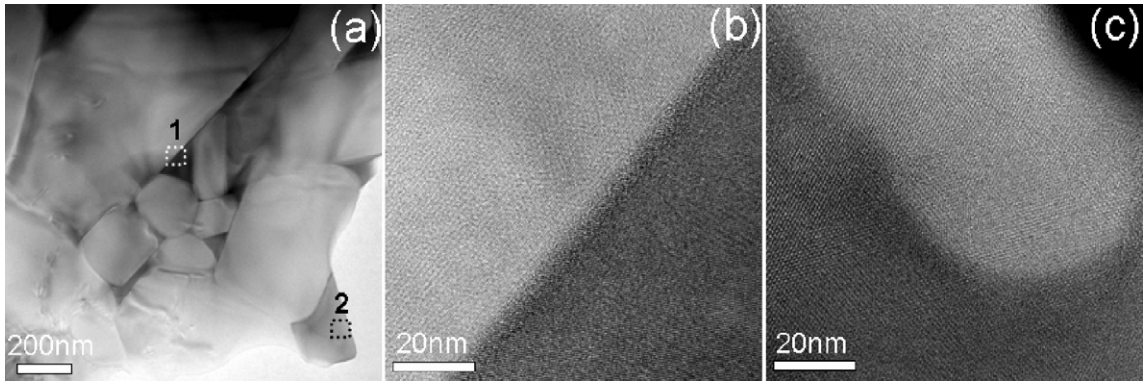

Fig. 6. (a) Representative TEM-BF image of heat treated Y–Sm–Ca doped SiAlON sample, (b) and (c) lattice-fringe images of crystalline secondary phase acquired from regions coded as "1" and "2", as seen by dashed line in panel (a).

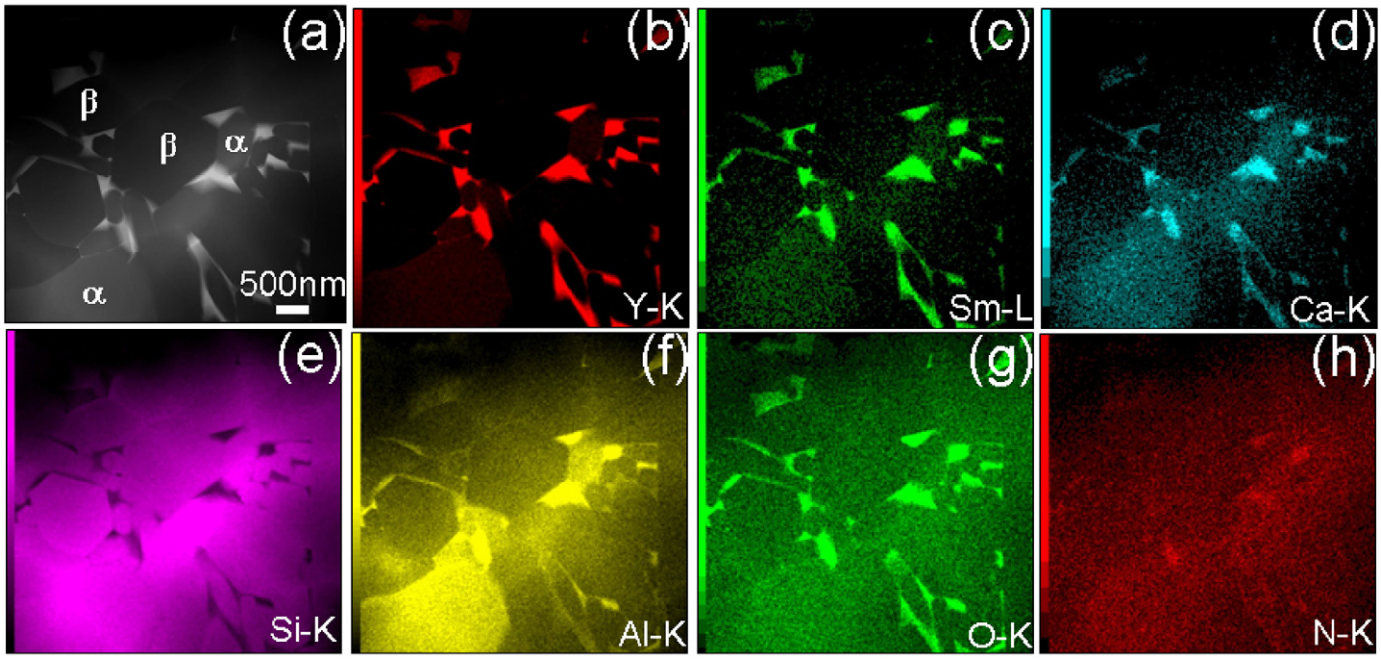

Fig. 7. (a) STEM-HAADF image of heat treated Y–Sm–Ca doped SiAlON sample, (b)–(h) STEM-EDX elemental mapping collected from characteristic X-ray lines of Y–K (b), Sm–L (c), Ca–K (d), Si–K (e), Al–K (f), O–K (g), and N–K (h).

images in Figure 5(b) and (c), we can elucidate that some of the quadruple junctions of sintered Y–Sm–Ca doped SiAlON sample is quite well-crystallised, resulting with formation of M' phase. This is further confirmed by fast Fourier transform (FFT) images given as inserts in Fig. 5(b) and (c) that junction in Fig. 5(b) is crystalline whereas in Fig. 5(c) is amorphous. In order to show the effect of heat-treatment on the crystallisation degree of secondary phases existing at triple and quadruples points, seen by dashed line and coded with "1" and "2" in Fig. 6(a), lattice-fringe images obtained from both regions and given in Fig. 6(b) and (c). The images confirm the increase of secondary phase crystallisation after heat treatment.

Moreover, for precise understanding of each sintering additives qualitative role on heat-treated SiAlON sample, the analytical findings obtained from Z-contrast STEM-HAADF imaging and X-ray elemental mapping combination are presented in Fig. 7(a)–(h). The results point out that the sintering additives (Y, Sm and Ca) appear mostly in compositions of amorphous and/or crystalline secondary phases and some incorporated into α-SiAlON (Fig. 7(b)–(d)). Although cations were detected in α-SiAlON grains by using the TEM-EDX point analysis[19,20] and in β-SiAlON grains by using the Z-contrast atomic resolution STEM imaging,[21] to the best of our knowledge, no study has been available so far to show that all the sintering additives (Y + Sm + Ca) used in this study were detected both in α-SiAlON grains and crystalline M' phase.

3.3. Mechanical properties

Although the microstructural features and the nature of intergranular phases are different depending on the applied heat treatment schedule and different dopant combinations, the mechanical properties are almost similar (Table 1). The hardness and indentation fracture toughness values of sintered and heat treated samples were found to lie in the range of 15.57–16.00 GPa and 5.43–5.89 MPa $m^{1/2}$ respectively (Table 1). The small differences in hardness values related to phase assemblage and M' phase content. Increase in the amount of α-SiAlON phase and M' phase generally leads to increase in hardness.

In SiAlON ceramics, the effect of interfacial properties is rather different than Si_3N_4 ceramics since some Al^{3+} cations enter into the crystal structure and also remain in the intergranular phase. Therefore, stronger interfacial bond exist between grain and intergranular phase in SiAlONs in comparison to Si_3N_4 ceramics.

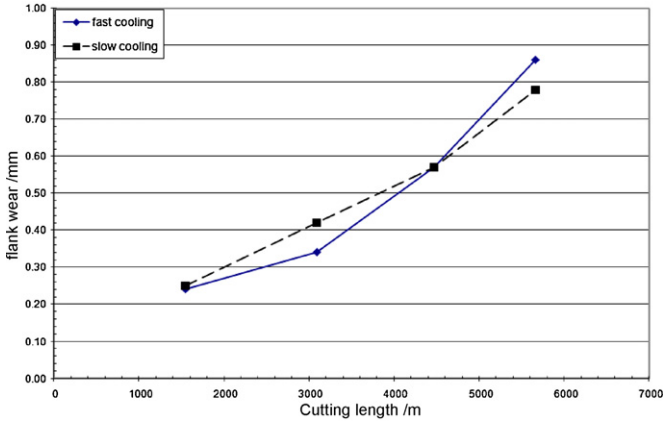

Fig. 8. Comparative machining test results of an Y-containing SiAlON after fast and slow cooling, respectively.

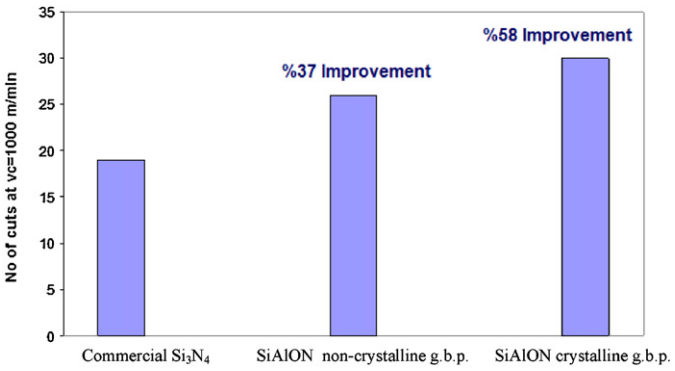

Fig. 9. Performance of a Y-rich SiAlONs with amorphous (fast cooled) or mostly crystalline grain boundary (heat treated) in comparison to a commercial silicon nitride material.

3.4. Machining performance

Fast cooled, slow cooled and heat treated SiAlON samples were tested against a commercial Si_3N_4 cutting tools under flank and notch wear conditions and the results are given in Figs. 8 and 9. It is found that flank wear of slow cooled samples are slightly better (10–15%) than fast cooled samples in the standart test conditions (Fig. 8). However, this difference is less than expected since more and significant amount of M^1 phase was detected after slow cooling (Fig. 2). One possible explanation is that machining conditions are not so severe to create a big difference.

In a further machining test, fast cooled and heat-treated SiAlON ceramics were tested on a high alloyed cast iron and compared to a commercial Si_3N_4 cutting tool (Fig. 9). In this particular test, chemical wear is the dominant wear mechanism, which results in a strong notch wear. The developed SiAlON ceramics generally showed a better cutting performance in comparison to commercial Si_3N_4 cutting tool due to the higher hardness of the SiAlONs (Fig. 9). A crystalline intergranular phase further improved the cutting performance around 58% compared to that of the Si_3N_4 material. Basically, heat treatment causes a reduction in the total surface area of the triple junctions and also promotes crystallisation. Increased crystallinity and coalescence of the intergranular phase is effective to reduce the chemical reaction tendency of the cutting tool with the work piece, resulting in less wear. It is also important to note that the creep resistance can also play a role on the better performance and it was found that the heat treated samples have much better creep resistance in comparison to as received samples.[22]

4. Conclusions

SiAlON ceramics with an α:β-ratio of 25:75 were designed with different molar ratios of Y:Sm:Ca as multi cation dopants. Combination of XRD and TEM analysis showed the existence of different amount of crystalline and amorphous phases depending on molar ratio, sintering conditions and heat treatment procedure. For example, M^1 phase was crystallised after slow cooling in 9Y:0.5Sm:0.5Ca system while amorphous intergranular phase was detected after fast cooling. Increase in Sm content from 5 to 60 mol% in Y–Sm–Ca system, very strong M^1 phase crystallisation was achieved even after fast cooling because of the lower eutectic temperature and nitrogen solubility in the Sm–Si–Al–O–N system. Slow cooling has similar effect to heat treated samples in terms of the amount of M^1 phase crystallisation. Heat treatment not only resulted in more intense crystallisation but also to a coarsening of the microstructure and a coalescence of the intergranular phase. 2 h heat treatment is enough to obtain crystalline intergranular phase at 1600 °C. Finally, machining tests showed that the life time of SiAlONs containing crystallised secondary phase (slow cooled or heat treated) is higher than that of SiAlON containing amorphous phase (fast cooled) and Si_3N_4 under chemical attack conditions since the difference is more pronounced in notch wear than flank wear. In conclusion, in this study, it is shown that crystalline secondary phases along with bigger grain size are necessary for improved machining performance of SiAlONs for further wide spread of use.

Acknowledgement

The authors wish to acknowledge the financial support of the Turkish Scientific and Technological Research Council in the scope of TUBITAK-TEYDEB-3040287 Project.

References

1. Satet RL, Hoffmann MJ. Impact of the intergranular film properties on microstructure and mechanical behaviour of silicon nitride. *Key Eng Mater* 2004;**264-268**:775–80.
2. Ziegler A, Kisielowski C, Hoffmann MJ, Ritchie RO. Atomic resolution transmission electron microscopy of the intergranular structure of a Y_2O_3 containing silicon nitride ceramics. *J Am Ceram Soc* 2003;**86**: 1777–85.
3. Shibata N, Pennycook SJ, Gosnell TR, Painter SG, Shelton WA, Becher P. Observation of rare earth segregation in silicon nitride ceramics at sub nanometre dimensions. *Nature* 2004;**428**:730–3.
4. Li YW, Wang PL, Chen WW, Cheng YB, Yan DS. Formation behaviour, microstructure and mechanical properties of multi-cation alpha SiAlONs containing calcium and neodymium. *J Eur Ceram Soc* 2001;**21**: 1273–8.
5. Liu M, Nasser SN. Microstructure and boundary phases of in-situ reinforced silicon nitride. *Mater Sci Eng* 1998;**A254**:242–52.
6. Li Y-W, Wang P-L, Chen W-W, Cheng Y-B, Yan D-S. Effect of additives on microstructure of Ca α-SiAlON. *Mater Lett* 2001;**47**:281–5.
7. Satet RL, Hoffmann MJ, Cannon RM. Experimental evidence of the impact of rare-earth elements on particle growth and mechanical behaviour of silicon nitride. *Mater Sci Eng A* 2006;**422**:66–76.
8. Painter GS, Becher PF, Shelton WA, Satet RL, Satet MJ. First-principles study of rare-earth effects on grain growth and microstructure of β-Si_3N_4 ceramics. *Phys Rev B* 2004;**70**:144–8.
9. Becher PF, Painter GS, Shibata N, Lin HT, Ferber MK. Macro- to atomic-scale tailoring of Si_3N_4 ceramics to enhance properties. *Key Eng Mater* 2005;**287**:233–41.
10. Acikbas NC, Kara A, Turan S, Kara F, Mandal H, Bitterlich B. Influence of type of cations on intergranular phase crystallisation of SiAlON ceramics. *Mater Sci Forum* 2007;**554**:119–22.
11. Mandal H, Kara F, Turan S, Kara A. Multication doped α-β-SiAlON ceramics, US Patent, 2004/0067838A1.
12. Gazzara CP, Messier DR. Determination of phase content of Si_3N_4 by X-ray diffraction analysis. *Am Ceram Soc Bull* 1977;**56**:777–80.
13. Evans AG, Charles EA. Fracture toughness determinations by indentation. *J Am Ceram Soc* 1976;**59**:371–2.

14. Mandal H, Heat treatment of SiAlON ceramics, PhD. Thesis, University of Newcastle Upon Tyne, 1992, p.149.
15. Camuscu N, Thompson DP, Mandal H. Effect of starting composition, type of rare earth sintering additive and amount of liquid phase on alpha-beta SiAlON transformation. *J Eur Ceram Soc* 1997;**17**:599–613.
16. Cao GZ, Metselaar R. α-SiAlON ceramics: a review. *Chem Mater* 1991;**3**(2):242–52.
17. Mandal, Thompson H, Reversible DP. α → β phase transformation in heat treated SiAlON ceramics. *J Eur Ceram Soc* 1993;**12**:421–9.
18. Thompson DP. Alternative grain-boundary phases for heat-treated Si_3N_4 and β-SiAlON. *Br Ceram Proc* 1990;**45**:1–13.
19. Turan S, Mandal H, Kara F. Transmission electron microscopy of SrO containing multi-cation doped α-SiAlON ceramics. *Mater Sci Forum* 2002;**383**:37–42.
20. Turan S, Mandal H, Kara F, Knowles KM. Transmission electron microscopy studies of La_2O_3-doped alpha-SiAlON ceramics. *Inst Phys Conf Ser* 1999;**161**:417–20.
21. Yurdakul H, Idrobo JC, Pennycook SJ, Turan S. Towards atomic scale engineering of rare-earth doped SiAlON ceramics through aberration corrected scanning transmission electron microscopy. *Scr Mater* 2011;**65**:656–9.
22. Uludag A, Turan D. High temperature bending creep behavior of a multi-cation doped α/β-SiAlON composite. *Ceram Int* 2011;**37**:921–6.